Measurement of mass, density, and volume during the cell cycle of yeast

Andrea K. Bryan[a,b], Alexi Goranov[b], Angelika Amon[b,c], and Scott R. Manalis[a,b,1]

[a]Department of Biological Engineering, [b]David H. Koch Institute for Integrative Cancer Research, and [c]Howard Hughes Medical Institute, Massachusetts Institute of Technology, Cambridge, MA 02139

Edited by Marc W. Kirschner, Harvard Medical School, Boston, MA, and approved December 7, 2009 (received for review February 19, 2009)

Cell growth comprises changes in both mass and volume—two processes that are distinct, yet coordinated through the cell cycle. Understanding this relationship requires a means for measuring each of the cell's three basic physical parameters: mass, volume, and the ratio of the two, density. The suspended microchannel resonator weighs single cells with a precision in mass of 0.1% for yeast. Here we use the suspended microchannel resonator with a Coulter counter to measure the mass, volume, and density of budding yeast cells through the cell cycle. We observe that cell density increases prior to bud formation at the G1/S transition, which is consistent with previous measurements using density gradient centrifugation. To investigate the origin of this density increase, we monitor relative density changes of growing yeast cells. We find that the density increase requires energy, function of the protein synthesis regulator target of rapamycin, passage through START (commitment to cell division), and an intact actin cytoskeleton. Although we focus on basic cell cycle questions in yeast, our techniques are suitable for most nonadherent cells and subcellular particles to characterize cell growth in a variety of applications.

biosensor | cell growth | cell size | microfluidics | Saccharomyces

Accurate measurements of cell size are fundamental to understanding the cell cycle and to identifying cell type and cell state. During exponential growth, cells require coordination between growth and division to maintain the population's size distribution, but it remains unclear how cells monitor and regulate cell cycle entry in response to cell size. The key to cell cycle control is the concentration of critical regulatory proteins, which is defined not only by expression levels, but the volume of the cell. Furthermore, cell volume is coupled to mass and energy requirements that control cell division and survival. Changes to rates of mass and volume accumulation may be correlated with cell cycle position and can be measured as variations in cell density. Yet even for model systems, such as the budding yeast *Saccharomyces cerevisiae*, these cellular-level parameters remain poorly investigated mainly because of a lack of tools for directly and accurately measuring cell mass or density.

Current methods for measuring cell density are limited to indirect measurements and density gradients, which can yield conflicting results. The density of fission yeast has been reported as cell cycle-dependent via interferometry (1) and cell cycle-*independent* via density gradient centrifugation (2). It is reported in ref. 2 that excessive sample manipulation may have influenced the interferometric results. Even so, measurements in density gradients can be complicated by possible interactions between the cells and the gradient medium (3, 4). Density measured by gradient centrifugation has been reported as cell cycle-independent during the CHO (5) and murine cell cycles (6), either independent or dependent on the *Escherichia coli* cell cycle (4, 7, 8), and cell cycle-dependent for budding yeast (9, 10). Studies using density gradient centrifugation have suggested that the changing density of budding yeast may correlate with bud formation (2, 11) or cyclic changes in water content and vacuole dynamics (10). Although more than one factor likely contributes to cell cycle-dependent density variation (or lack thereof) across cell types, mechanisms that give rise to density variation in budding yeast may be conserved in other eukaryotes.

The ideal density measurement would directly monitor the mass and volume of each cell within a population with minimal sample perturbation and allow cells to be collected for subsequent measurements. Toward this aim, we utilized the suspended microchannel resonator (SMR) to measure single-cell buoyant mass with high precision. The SMR is a silicon cantilever with an embedded microfluidic channel that resonates at a frequency proportional to its total mass, which changes as individual cells flow through the channel (Fig. 1) (12). We measured density in two ways with the SMR. The first provides an alternative to density gradient centrifugation and population-based approaches described previously (13) by measuring buoyant mass with the SMR and, on the same sample, volume with a commercial Coulter counter. Unlike density gradient centrifugation, this technique provides buoyant mass and volume information, measures growth-arrested cells in almost any medium, and does not require density gradient chemicals. With this method we found that cell density increases prior to bud formation at the G1/S transition. To investigate the origin of this density increase, we used the SMR in a second method where relative density changes of growing yeast cells are measured as the cells are sampled by the microchannel. We found that the density increase requires energy, passage through START, function of the protein synthesis regulator target of rapamycin (TOR), and an intact actin cytoskeleton. In conjunction with these density measurements, FACS analysis and bud emergence data suggest that this density change is independent of DNA replication and may result from several START-dependent events.

Results and Discussion

Density, Volume, and Buoyant Mass of Growth-Arrested Cells. Cell buoyant mass, volume, and density were measured by combining the SMR's buoyant mass readout with a commercial Coulter counter's volume measurements. Buoyant mass is the change in cantilever mass as a cell transits the channel or the difference between the mass of the cell and the mass of the displaced fluid. The relationship between a cell's buoyant mass and the fluid density is linear, and the slope of this line is related to the cell volume (Fig. 2). Cell density can be extrapolated from this line as the point at which buoyant mass is zero or at which fluid density exactly matches cell density. For populations, the flow-through configuration of the SMR allows cells to be collected during the buoyant mass measurement and used in downstream measurements for paired data analysis, such as volume, but this yields relatively few cells ($n < 3000$). Volume measurements ($n > 20,000$) recorded before the sample was loaded in the SMR were used in

Author contributions: A.K.B., A.G., A.A., and S.R.M. designed research; A.K.B. and A.G. performed research; A.K.B., A.G., A.A., and S.R.M. analyzed data; and A.K.B., A.G., A.A., and S.R.M. wrote the paper.

The authors declare no conflict of interest.

This article is a PNAS Direct Submission.

[1]To whom correspondence should be addressed. E-mail: scottm@media.mit.edu.

This article contains supporting information online at www.pnas.org/cgi/content/full/0901851107/DCSupplemental.

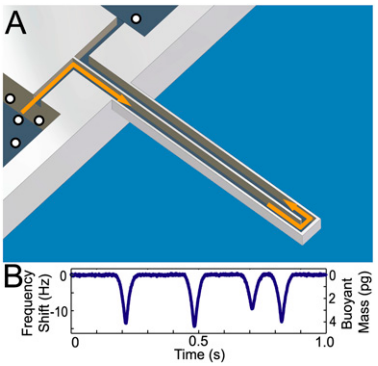

Fig. 1. Illustration of instrument and cell measurement. (*A*) The cantilever vibrates in and out of plane with an amplitude of a few hundred nanometers. Cells flowing through the vibrating cantilever microchannel displace a volume of fluid equal to their own volume and, at a given position, change the cantilever's resonant frequency proportional to this change in cantilever mass. The flow rates are controlled by pressure. The number of single-cell measurements was maximized by adjusting the sample concentration. A more detailed description of the instrument and its operation is available in ref. 12. (*B*) The frequency shift as cells flow through the microchannel (four of which are shown) is position-dependent, and the maximum frequency shift, which is proportional to the recorded buoyant mass, occurs when the cell is at the cantilever tip. The frequency returns to baseline upon each cell's exit from the cantilever.

the density calculation. In this way buoyant mass and volume measurements are made with the same sample, the data are pooled into buoyant mass and volume histograms, and each histogram is fit to a log-normal function. To calculate the density of a cell population, the means of the fitted functions are substituted into $\rho = \rho_f + m_B/V$, where ρ is the cell density, ρ_f is the fluid density, m_B is the buoyant mass, and V is the cell volume. For comparisons between samples, the cell buoyant mass was adjusted for the fluid density of water at 20 °C (0.9982 g/mL) by $m_B = m_{B,\text{measured}} + (\rho_f - \rho_{\text{water},20\,^\circ\text{C}}) \cdot V$.

This technique was verified with 3.67 ± 0.1 μm diameter National Institute of Standards and Technology particle size standards. The beads have a mean 1.38 ± 0.010 pg buoyant mass in water ($T \sim 20$ °C, fluid density = 0.9980 g/mL) and a 27.0 ± 0.10 μm^3 mean volume. We calculated the density of the particles to be 1.0486 ± 0.0010 g/mL, which is in accordance with the accepted polystyrene density of 1.05 g/mL. Errors in both the volume and mass parameters contribute to this density calculation. The Coulter counter's error results from inherent instrument noise. The SMR's main source of error is variation in particle position at the cantilever tip. Position variation contributes ~6% to the measurement's uncertainty for a 3.67-μm diameter particle, slightly less than the inherent size deviation of the population. This error decreases with increased particle diameter and is generally not significant for populations with larger size variation, such as cells. The SMR also has a relatively low throughput compared to the Coulter counter. For National Institute of Standards and Technology particle standards we recorded >300 SMR measurements in <30 min, and for cell samples we recorded >1,500 SMR measurements in <1 hr. For both particle standards and cells, >20,000 Coulter counter measurements were recorded in <1 min.

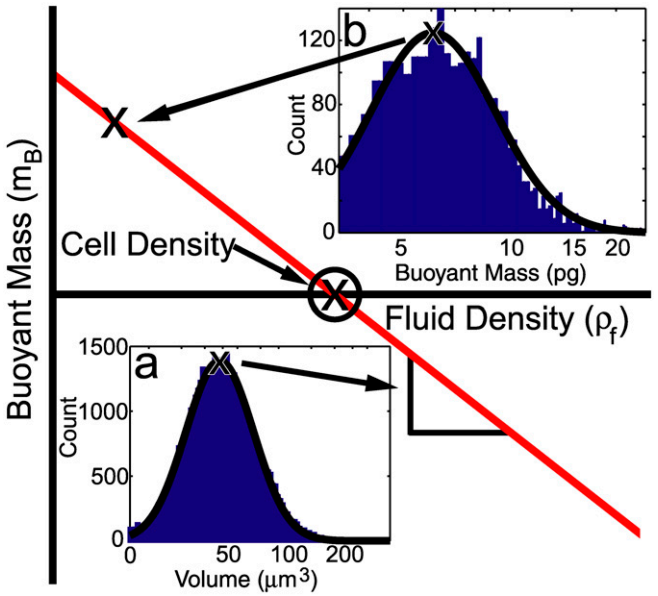

Fig. 2. Cell density, mass, and volume measurements. Cell density is calculated by the linear relationship between buoyant mass and fluid density (red line, equation in text). The slope of this line is determined by the cell volume (*Inset A*) and is measured by a commercial Coulter counter on the same sample loaded in the SMR. The buoyant mass (*Inset B*) is determined by a distribution of >1500 SMR measurements. An example of four of these measurements made in phosphate buffer is in Fig. 1*B*. The means of the fitted log-normal functions (X on *Insets*) are used to calculate average cell density.

Yeast Density and Growth Rates are Coordinated with the Cell Cycle. The yeast cell cycle is a highly regulated series of events controlled by the activation of cyclin-dependent kinases (CDKs) by cyclins. CDK activation drives cell cycle progression, and it is suggested that the expression level of a certain cyclin, Cln3, serves to coordinate size, mass, and volume, with entry into the cell cycle (14). The point at which cells commit to cell cycle entry is called the START or restriction point (15). To determine how cell density correlates with the cell cycle, we measured the distributions of buoyant mass and volume in budding yeast populations. The density of asynchronous budding yeast in our strain background, W303, was 1.1029 ± 0.0026 g/mL (Fig. 3*A*), slightly lower than the density of 1.1126 g/mL reported by density gradient centrifugation in the Y55 strain (10). Because cells are not uniformly distributed through the cell cycle in an asynchronous population (~80% of W303 cells are in the S or M phase, estimated by budded cell counts), this density is expected to be weighted by the time cells spend in each phase of the cell cycle. We next measured the buoyant mass, density, and volume of cells arrested in various stages of the cell cycle. The density of cells arrested in G1 by treatment with the pheromone alpha factor decreased 1.7% to 1.0846 ± 0.0043 g/mL. The decrease in G1 density was also observed in cells arrested by using the analog-sensitive CDK mutant *cdc28-as1*. This allele responds to the ATP analog 1-NM-PP1, which produces a G1 arrest by selectively occupying the modified ATP binding pocket of *cdc28-as1* and inhibiting CDK activity (16). Cells arrested in G1 via *cdc28* inactivation (pp1) had a density of 1.0812 ± 0.0100 g/mL, a 2% decrease from the 1.1034 ± 0.0022 g/mL density of asynchronous *cdc28-as1* populations. Despite the longer arrest (3 hr) and larger cell volume (Fig. 3*B*), arrested *cdc28-as1* cells had a density similar to that of a 2-hr alpha-factor arrest, which may indicate well-matched mass and volume growth rates between these G1 arrests. The density of cells arrested in S phase by the replication inhibitor hydroxyurea was 1.1049 ± 0.0024 g/mL, approximately the same as the asynchronous population. S-phase arrested cells could be expected to have a higher density on the basis of previous findings (9, 10), and our result may be an effect of the drug or indicate differences between S-phase arrested cells and those in an asynchronous population. The density of cells arrested in metaphase by the microtubule inhibitor nocodazole (NOC) was 1.0998 ± 0.0049 g/mL, or ~1.5% decrease from the mock-treated (DMSO) asynchronous culture density of

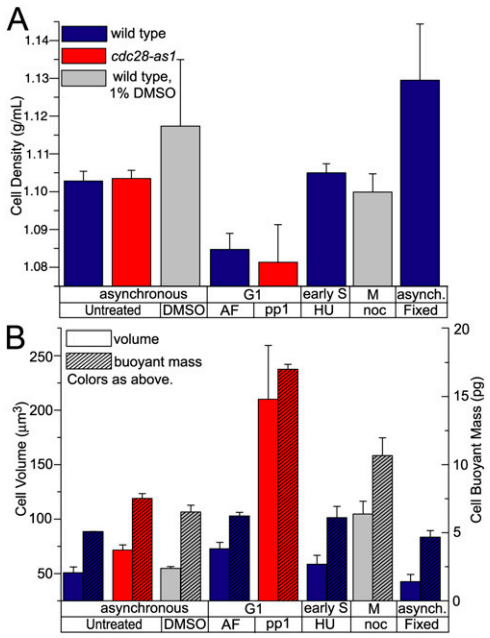

Fig. 3. Density, buoyant mass, and volume of cells synchronized by cell cycle blocks. (*A*) WT (A2587) and *cdc28-as1* (A4370) densities (mean ± SD) in arrested G1 and metaphase are lower than asynchronous mock-treated (untreated, DMSO) populations. The density of the asynchronous population is approximately the same as S-phase arrested cells and reflects the unequal distribution of cells throughout the cell cycle. Cells were synchronized with alpha factor (AF) for 2 hr (5 μM), 1-NM-PP1 (pp1) CDK inhibitor for 3 hr (5 μM), hydroxyurea (HU) for 2 hr (10 mg/mL), and nocodazole (NOC) for 2 hr (15 μg/mL), as indicated. Fixed cells were fixed in 3.7% formaldehyde for various amounts of time. (*B*) Buoyant mass ($\rho_f = \rho_{water,20\,°C}$) and volume measurements for the same cell populations (mean ± SD).

1.1173 ± 0.0176 g/mL. These results suggest that density for arrested populations is cell cycle-dependent, which further supports the findings by others (9, 10) that density is regulated by cell cycle progression.

Because the differences in density could be artifacts of the different treatments or the cell cycle arrests, we sought to determine if cell density varied during an unperturbed cell cycle. For this purpose we measured the buoyant mass, volume, and density of G1 cells isolated by centrifugal elutriation, resuspended in media for synchronous cell cycle progression, and formaldehyde-fixed overnight. Although fixation artificially increases cell density (Fig. 3*A*), the relative density throughout the time course (Fig. 4*A*) agrees with our previous observations and others' (9, 10). Cell density was correlated with cell cycle position by comparing the cell density with the percent of budded cells (Fig. 4*A*, numbers in brackets). The density is relatively low in elutriated G1 (unbudded) cells, increases to near maximum during late G1 and S-phase entry (bud formation), and then decreases through mitosis. The recorded cell density does not return to its minimum at the end of the first cell cycle because of the time course's resolution, loss of synchrony, or a possible elutriation effect on the initial selection. Buoyant mass and volume continue to increase throughout the time course as the cells grow and the population adjusts from the elutriation's size selection (Fig. 4*B*).

Although the density of arrested cells can be calculated with high precision because buoyant mass and volume are measured over an extended period, this limits the temporal resolution and makes it difficult to observe growth dynamics. In order to address this limitation and to measure an uninterrupted cell cycle, we continuously sampled from split cultures of elutriated G1 yeast cells that remained in media for both measurements. Buoyant mass and volume growth rates increase during the cell cycle,

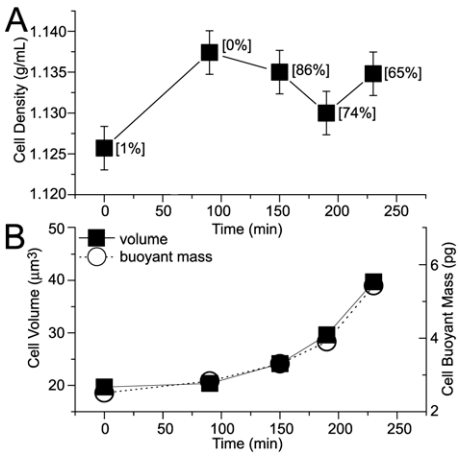

Fig. 4. Density, buoyant mass, and volume of cells synchronized by elutriation. (*A*) Density of formaldehyde-fixed-cell populations (A11311) grown overnight in YEP + 2% raffinose and a synchronized sample was selected by centrifugal elutriation. Bud counts are reported as percent budded in brackets next to each measurement. Cells begin to enter S phase between 60 and 120 min. Error bars are the SEM measured with a single fixed sample of elutriated WT cells (A11311, $n = 3$). (*B*) Buoyant mass ($\rho_f = \rho_{water,20\,°C}$) and volume increase throughout the time course. Changes in cell density at the population level are the result of differences in the relative rates of mass and volume increase through the cell cycle.

and the coefficient of variation for volume is greater than that observed in buoyant mass (Figs. 5 and S2–S4). The distributions widen as the culture loses synchrony and cell size variation emerges. Although the smaller sample size prevented accurate density calculations, this approach offers a powerful means to observe growth dynamics in synchronized cell populations.

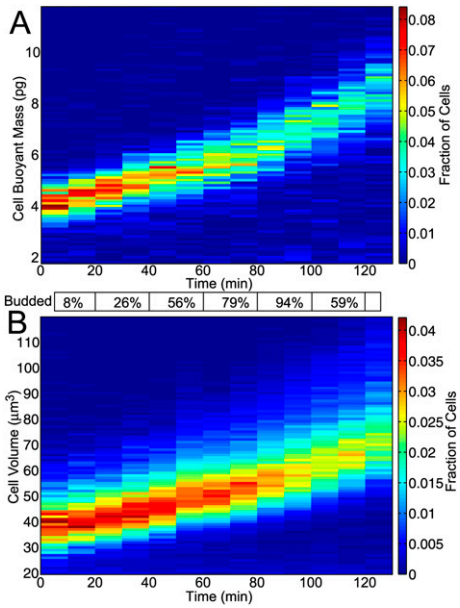

Fig. 5. Buoyant mass and volume growth rates are cell cycle-dependent. Color designates the fraction of the population with the indicated buoyant mass and volume (color bar at right). Small unbudded cells (A2587) were isolated by elutriation for synchronous culture after overnight growth in YEPD, which partially reduced synchrony. (*A*) The SMR steadily sampled from the culture and measurements were broken into 10-min divisions ($n = 7,839$ cells). (*B*) Volume measurements on a split culture were made from aliquots drawn at 10-min intervals and recorded in <1 min ($n = 67,607$ cells). Additional budding data is available in Fig. S1.

In summary, our data show budding yeast increase density prior to bud formation and increase volume and buoyant mass growth rates throughout the cell cycle. The density increase may result from several START-dependent events, and to investigate this we have developed a method that enables cell density to be measured in real time for unperturbed cells.

Relative Density Measurement of Single Cells During Growth. The SMR reads out real-time changes in relative cell density via the direction of change in buoyant mass as synchronized and growing cells flow through the cantilever. A cell with a density greater than that of the fluid appears as a positive buoyant mass, and a cell with a density less than that of the fluid appears as a negative buoyant mass (Fig. 6). If the media density is adjusted to be between the initial and final cell densities, then the ratio of the positive to total number of measurements in a short time (1 min) approximates the fraction of cells in the higher density state at that time. This single-cell technique enables the timing and detection of density changes in biological samples as they occur in growth media. It has a higher time resolution than current gradient-based approaches and does not involve a subsequent gradient fractionation to define the density distribution (7). This method may also be applied to cells transitioning to lower density by decreasing the fluid density to below that of the cells' initial density.

The precision of this technique relies on the method for modifying the fluid density, the SMR's resolution, and the degree of overlap in the density distributions of the two cell states. To modify the density of YEPD (yeast extract/peptone supplemented with 2% glucose) we selected Percoll (Sigma-Aldrich), a colloidal silica suspension, for its low osmolality, low viscosity, and general impermeability of biological membranes (17). Experiments with Histodenz (Sigma-Aldrich) showed density changes for arrested yeast, likely through an osmotic response, such as is observed in bacteria (18). The resolution of the 8-μm-tall SMR used for these experiments is ~3 fg (1-Hz bandwidth). This can detect a 0.1% yeast density change in a high-density solution, and we measured ~2% change through the cell cycle. By measuring trends in synchronized populations, sample number increases and the method's statistical precision and reproducibility further improves.

The G1/S Density Change in Yeast. We used this method to further investigate cell density changes in yeast and how density is coupled to the G1/S transition. Changes in density are indicative of differences between rates of total mass and volume increase, which may be correlated to specific cell cycle events. Cells were first synchronized via alpha factor and released into a YEPD:Percoll media (fluid density ~1.086 g/mL), and as the cells progressed through the cell cycle they were continuously flowed through the SMR for single-cell buoyant mass measurements over a time course. As cells neared S-phase entry and became denser, the proportion of cells with a density above that of the fluid increased (Fig. 7, mock-treated release). This shift demonstrates that alpha-factor treatment arrests cells before the density increase observed in the unperturbed cell cycle of G1 elutriated cells. The shift is consistently observed following alpha-factor release, but the kinetics are not always identical. The timing and rate of this density shift depends on the cell treatment, efficiency of release, and the difference between cell and media density. If the difference between the cell and media densities varies between experiments, then the timing of the density change, the point at which the cell density is greater than that of the media, will also vary. These variances are responsible for the differences in mock-treated WT behavior observed during the experiments of Fig. 7. Although the technique is not suitable for quantifying density, it does enable the real-time detection of relative density changes that occur near the media density and, by the rate of transition, provides some information regarding population synchrony.

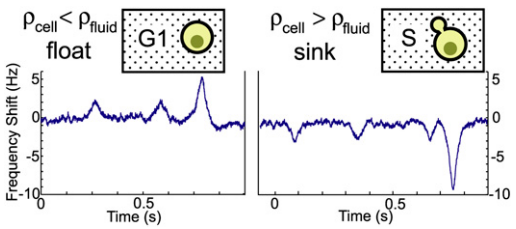

Fig. 6. Real-time relative cell density measurement. Cell state, distinguished by cell density, is determined by the cell's direction of frequency shift in media with a density slightly above that of G1 cells. G1-synchronized cells have a negative buoyant mass (positive frequency shift), and cells entering S phase at a later time point have a positive buoyant mass (negative frequency shift). The proportion of cells in each state is directly correlated to the percent of cells below or above fluid density and changes as cells synchronously progress through the cell cycle.

The Change in Yeast Density at G1/S Requires Energy, TOR function, START, and an Actin Cytoskeleton. To characterize the yeast density shift at the G1/S transition as an energy-dependent process, we blocked ATP synthesis with sodium azide, an inhibitor of F_1-ATPase, immediately following release from an alpha-factor arrest. The SMR's buoyant mass measurements detected a cell density change in mock-treated control cells and no change in density for cells treated with azide (Fig. 7*A*). Thus, the density change we previously observed is an active process requiring ATP.

The TOR pathway controls translation initiation and stimulates protein synthesis in response to nutrients (19). To examine whether the density shift depends on protein synthesis, we asked whether the TOR pathway was required. We treated cells released from an alpha-factor-induced arrest with rapamycin, an inhibitor of TORC1 function (20), and compared the percent

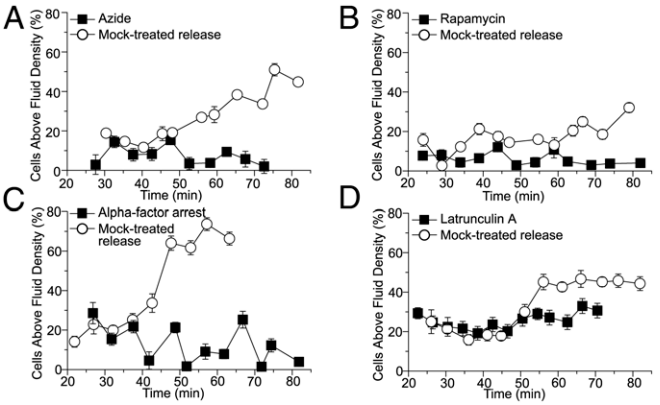

Fig. 7. Changes in cell density require energy, TOR function, passage through START, and an intact cytoskeleton. WT cells (A2587) were arrested in alpha factor and released in YEPD:Percoll media with each treatment. Increases in the percent of cells with a density above that of the fluid signify an overall increase in cell density. (*A*) Azide (0.1% wt/vol) prevented the density change and demonstrates an energy requirement for the density increase. Mock-treatment: equal volume water. (*B*) Rapamycin (10 μM) prevented the density change and establishes a TOR function requirement. Mock-treatment: equal volume 70% ethanol. (*C*) Alpha factor (5 μM) prevented the density change and confirms a passage through START requirement. Mock-treatment: equal volume DMSO. (*D*) LatA (100 μM) prevented the density change and establishes a requirement for an intact actin cytoskeleton. Mock-treatment: equal volume DMSO. Error bars are the standard error of the proportion. The Bonferonni-corrected significance for each treatment was $p \sim 0.01$ for (*A*), $p \sim 0.05$ for (*B*), $p \sim 0.04$ for (*C*), and $p \sim 0.06$ for (*D*).

of cells with a change in density to the resulting percentages for a parallel-grown mock-treated control culture. Cells from the control culture changed in density, and cells with TOR inactivation did not change in density (Fig. 7*B*). Thus, the change requires TOR function and, likely, protein synthesis.

To determine whether START is required for the density change, we prolonged a G1 arrest via continuous treatment with alpha factor. Mock-treated cells released into fresh YEPD changed in density, and cells that were resuspended in alpha-factor-containing medium displayed no significant change in density during an 85-min time course (Fig. 7*C*). These results suggest that the density shift is START-dependent but do not indicate whether it results from bud formation, DNA replication, or some other START-dependent process.

Bud formation requires polarization of the actin cytoskeleton, and we investigated the possibility that the actin cytoskeleton has a function in the cell density increase. We treated cells released from an alpha-factor arrest with an inhibitor of actin polymerization, latrunculin A (LatA). We measured a change in density for mock-treated control cells and no change in density following LatA treatment (Fig. 7*D*). We also monitored bud appearance for similarly treated cells and confirmed that the LatA treatment severely inhibited bud formation (Fig. S5*A*). Thus, disruption to the actin cytoskeleton prevents the density change, which may be the direct effect of perturbing actin-dependent processes such as vesicular transport required for growth, or result from other LatA effects on cell growth (21).

To investigate if the density change also requires DNA replication, we examined DNA content by FACS analysis. Cellular DNA was fluorescently labeled and the distribution of relative DNA content (C, 2C) was measured for synchronized samples. The LatA and rapamycin treatments following release from an alpha-factor arrest reduced DNA replication by nearly the same amount (Fig. S5*B*). At 60 min, ~10% of the mock-treated and ~35% of the LatA- and rapamycin-treated cells exhibited 1C DNA, or had not yet replicated (Fig. S5*C*). The rapamycin treatment following release from an alpha-factor arrest also severely inhibited bud formation (Fig. S5*A*). Rapamycin is known to prevent entry into the cell cycle by inhibiting translation initiation (19); however, we have observed the effects of rapamycin to be more severe on budding than on replication. Rapamycin- and LatA-treated cells do not change in density and do not form buds but do replicate to a significant extent. Therefore, the change in density near the G1/S transition is independent of DNA replication, and inactivation of actin-related processes such as cell polarization, budding, and/or vesicular transport may inhibit pathways required for this density change.

Understanding the mechanism for this cell cycle-dependent density change is important in describing cell growth dynamics. A density change confirms that changes to total mass (protein synthesis, vacuolar dynamics) and volume increase (membrane growth) are not directly proportional, and the requirements for a density change at the G1/S transition of budding yeast demonstrate a coupling between these two processes. We have observed that perturbations to membrane growth early in the cell cycle, such as the inhibition by LatA of budding and growth, abolish changes in density, and previous studies have shown that protein synthesis is linked to membrane growth (22). A change in density, or differences between mass and volume rates of increase, may occur as a result of a transient increase to mass accumulation during polarized membrane growth at the G1/S transition, a slowdown in membrane expansion during coordination with bud formation, and/or changes to cell water content. One caveat in this hypothesis is that pheromone-treated cells, while polarized, remain low in density. However, this lower density may result from decreased protein synthesis and other effects of alpha-factor treatment (23). Another possibility is that changing vacuole size may alter density. Cln3 regulates vacuole size at the G1/S transition (24), and cells with larger vacuoles have decreased density (9). We have measured *vps*33Δ mutants (small, fragmented vacuoles) in the S288C background to have a density ~0.8% greater than the WT density of 1.1174 ± 0.0039 g/mL, as in ref. 11. However, analysis of the vacuole's role in cell cycle-dependent density changes is complicated by long cell cycle times in class I vacuole mutants, and thus little is known about how the vacuole affects cell density at the single-cell level and during a normal cell cycle.

Conclusions and Future Directions

We have presented mass, density, and volume measurements throughout the cell cycle and developed two unique measurement techniques to identify the density change in budding yeast at the G1/S transition as dependent on energy, TOR function, passage through START, and the actin cytoskeleton. One possible model for the density variation with these dependencies is one in which polarized growth enables processes during late G1 to increase cell density and changes in volume during bud formation at S phase decrease cell density. This linkage between mass and membrane growth is central to how the cell coordinates growth with division and may have an important role in the signal for cell cycle progression. The density measurement techniques may be generalized to other cells and subcellular particles, and future technology developments aim to acquire single-cell mass and density measurements at once and with only the SMR. This, combined with the ability to continuously monitor single cells, could detail the cell-to-cell variations that are otherwise obscured in population measurements and would provide the basis for a more complete understanding of cell growth, division, and response.

Materials and Methods

SMR Measurements. Devices and fluidic controls are as described in ref. 12 with the exception of a larger (~8 × 8 μm) cantilever channel cross-sectional area. Devices were further enlarged to ~9 × 9 μm by a KOH etch at 40 °C postfabrication. Cell volume was measured twice for the density measurement in the first method—once before the mass measurement and once on the sample of cells collected from the SMR waste channel—to pair the measurements and ensure that the measured cells were representative of the original sample.

Strains, Growth Conditions, and Sample Preparation. The yeast strains used in this study are listed in Table 1. Cells were grown in YEPD at room temperature (21 °C). Cells were synchronized with 5 μg/mL alpha factor at 0 and 90 min, for a total arrest of 120 min, with the exception of cells synchronized by the 120-min hydroxyurea (10 mg/mL) or nocodazole (15 μg/mL) treatment. An equal volume DMSO mock-treated culture was a control for the nocodazole measurements. For *cdc28-as1*, cells were arrested with 1-NM-PP1 (5 μM) for

Table 1. Yeast strains used in this study

Strain	Relevant genotype
A2587*	(WT) MATa, ade2-1, leu2-3, ura3, trp1-1, his3-11,15, can1-100, GAL, psi+
A4370*	MATa, cdc28-as1
A11311*	MATa, ade1::HIS3, lys2::KanMX
BY4741†	(WT) MATa, his3D1, leu2D0, met15D0, ura3D0
KO collection†	MATa, *vps*33Δ::KanMX.

*Strains in the W303 background.
†Strains in the S288C background.

3 hr. For the density measurements on growth-arrested cells, cells were washed via vacuum filtration at 120 min and concentrated in phosphate buffer to $\sim 10^8$ cells/mL. Volume was measured on a Multisizer 3 Coulter counter fitted with a 100-μm aperture tube, the sample was delivered to the SMR, and the cells were collected from the waste side of the SMR to be measured again with the Coulter counter. We observed no change in cell volume resulting from suspension in phosphate buffer. We compared the original sample volume distribution to that of cells collected from the SMR waste and directly observed the SMR's preferential selection of small particles. This bias was mitigated with higher flow rates.

For real-time sample preparation, cells were grown and arrested as described above. Cells were washed via vacuum filtration and concentrated in a 65:25:10 Percoll (Sigma-Aldrich): 4xYEPD:H2O solution to $\sim 10^7$ cells/mL. Depending on treatment, alpha factor (5 ug/mL), azide (0.1% wt/vol), rapamycin (10 μM), LatA (100 μM), DMSO, or ethanol control was added to the cell suspension. Cell volume was recorded by a Coulter counter and the sample was delivered to the SMR at room temperature.

Elutriation. Cells were grown overnight in YEP +2% raffinose for density measurements (Fig. 4) and YEPD for continuous measurements (Fig. 5), synchronized by centrifugal elutriation (25), and resuspended in YEPD. For continuous measurements the sample was concentrated and delivered to the SMR for mass measurement in media. Aliquots for fixed-cell density measurements were collected into 3.7% formaldehyde at indicated time points. Fixation was required for a complete cell cycle time course because the time required for the density measurement is much longer than the cell cycle. After fixation, cells were washed and resuspended in phosphate buffer, the volume distribution was recorded on the Coulter counter, and the sample was delivered to the SMR for mass measurement.

Flow Cytometric Analysis. Cells released from alpha-factor arrest were concentrated to $\sim 10^8$ cells/mL in a 1-mL volume and shaken in an angled test tube at 275 rpm. LatA (100 μM), rapamycin (10 μM), DMSO, or ethanol control was added to each culture, and 15-min time points were collected into 70% ethanol for 120 min. Samples were prepared and stained with propidium iodide as previously described (26).

Statistical analysis. Slopes for each of the real-time density experiments were calculated by linear regression. A one-way ANOVA test was performed on the slopes for the five groups (release from an alpha-factor arrest, azide, continuous alpha-factor treatment, rapamycin, LatA), each with $n = 3$. The release group consists of a control measurement for the azide, rapamycin, and LatA treatments. A Bonferonni-corrected t test for the individual treatments and the release group was used to report significance of each treatment (Fig. 7).

ACKNOWLEDGMENTS. We thank C. Gonzales for his separation of cells by centrifugal elutriation. This work was supported by the National Institutes of Health EUREKA (R01GM085457) and Center for Cell Decision Process grants (P50GM68762) (to S.R.M.), the National Institutes of Health Grant GM056800 (to A.A.), by a Postdoctoral Fellowship from the American Cancer Society (to A.G.), and by an NSF Graduate Fellowship (to A.K.B.). A.A is an investigator of the Howard Hughes Medical Institute.

1. Mitchison JM (1957) The growth of single cells I. Schizosaccharomyces pombe. *Exp Cell Res*, 13:244–262.
2. Kubitschek HE, Ward RA (1985) Buoyant density constancy of Schizosaccharomyces pombe cells. *J Bacteriol*, 162:902–904.
3. Pertoft H (2000) Fractionation of cells and subcellular particles with Percoll. *J Biochem Biophys Meth*, 44:1–30.
4. Kubitschek HE, Baldwin WW, Graetzer R (1983) Buoyant density constancy during the cell cycle of Escherichia coli. *J Bacteriol*, 155:1027–1032.
5. Anderson EC, Petersen DF, Tobey RA (1970) Density invariance of cultured Chinese hamster cells with stage of the mitotic cycle. *Biophys J*, 10:630–645.
6. Loken MR, Kubitschek HE (1984) Constancy of cell buoyant density for cultured murine cells. *J Cell Physiol*, 118:22–26.
7. Woldringh CL, Binnerts JS, Mans A (1981) Variation in Escherichia coli buoyant density measured in Percoll gradients. *J Bacteriol*, 148:58–63.
8. Poole RK (1977) Fluctuations in buoyant density during the cell cycle of Escherichia coli K12: Significance for the preparation of synchronous cultures by age selection. *J Gen Microbiol*, 98:177–186.
9. Hartwell LH (1970) Periodic density fluctuation during the yeast cell cycle and the selection of synchronous cultures. *J Bacteriol*, 104:1280–1285.
10. Baldwin WW, Kubitschek HE (1984) Buoyant density variation during the cell cycle of Saccharomyces cerevisiae. *J Bacteriol*, 158:701–704.
11. Ohsumi M, Uchiyama K, Ohsumi Y (1993) Density fluctuation during the cell cycle in the defective vacuolar morphology mutants of Saccharomyces cerevisiae. *J Bacteriol*, 175:5714–5716.
12. Burg TP, et al. (2007) Weighing of biomolecules, single cells and single nanoparticles in fluid. *Nature*, 446:1066–1069.
13. Godin M, Bryan AK, Burg TP, Babcock K, Manalis SR (2007) Measuring the mass, density, and size of particles and cells using a suspended microchannel resonator. *Appl Phys Lett*, 91:123121.
14. Rupes I (2002) Checking cell size in yeast. *Trends Genet*, 18:479–485.
15. Planas-Silva MD, Weinberg RA (1997) The restriction point and control of cell proliferation. *Curr Opin Cell Biol*, 9:768–772.
16. Bishop AC, et al. (2000) A chemical switch for inhibitor-sensitive alleles of any protein kinase. *Nature*, 407:395–401.
17. Pharmacia Fine Chemicals (1985) *Percoll. Methodology and Applications. Density Marker Beads for Calibration of Gradients of Percoll* (Pharmacia Fine Chemicals, Uppsala, Sweden).
18. Baldwin WW, Myer R, Powell N, Anderson E, Koch AL (1995) Buoyant density of Escherichia coli is determined solely by the osmolarity of the culture medium. *Arch Microbiol*, 164:155–157.
19. Crespo JL, Hall MN (2002) Elucidating TOR signaling and rapamycin action: Lessons from Saccharomyces cerevisiae. *Microbiol Mol Biol R*, 66:579–591 table of contents.
20. Heitman J, Movva NR, Hall MN (1991) Targets for cell cycle arrest by the immunosuppressant rapamycin in yeast. *Science*, 253:905–909.
21. Karpova TS, et al. (2000) Role of actin and Myo2p in polarized secretion and growth of Saccharomyces cerevisiae. *Mol Biol Cell*, 11:1727–1737.
22. Mizuta K, Warner JR (1994) Continued functioning of the secretory pathway is essential for ribosome synthesis. *Mol Cell Biol*, 14:2493–2502.
23. Goranov AI, et al. (2009) The rate of cell growth is governed by cell cycle stage. *Gene Dev*, 23:1408–1422.
24. Han BK, Aramayo R, Polymenis M (2003) The G1 cyclin Cln3p controls vacuolar biogenesis in Saccharomyces cerevisiae. *Genetics*, 165:467–476.
25. Amon A (2002) Synchronization procedures. *Methods Enzymol*, 351:457–467.
26. Hochwagen A, Tham WH, Brar GA, Amon A (2005) The FK506 binding protein Fpr3 counteracts protein phosphatase 1 to maintain meiotic recombination checkpoint activity. *Cell*, 122:861–873.